Evaluation of damage in composites by using Thermoelastic Stress Analysis: a promising technique to assess the stiffness degradation

Rosa De Finis[1,2], Davide Palumbo[2], and Umberto Galietti[2]

[1]Polytechnic Institute of Bari
[2]Politecnico di Bari

May 5, 2020

Abstract

The stiffness degradation represents one of the most interesting phenomena used for describing the fatigue behaviour of composites. In this regard, in literature, several works have been presented for modelling the fatigue life by studying the stiffness degradation. A critical aspect of modelling damage fatigue is represented by the difficulties in simulating the whole behaviour of material and then in describing the damage progression in all its stages. In addition, the validation of models requires the measurement of stiffness variations by means of experimental techniques. Above all for real components, the difficulties in defying proper models are accompanied by the difficulties in measuring stiffness degradation due to inapplicability of classic experimental techniques. In this work, the stiffness degradation of quasi-isotropic carbon-fibre-reinforced-polymer obtained by automated fiber placement, has been assessed by means of Thermoelastic Stress Analysis. The amplitude of temperature signal at the mechanical frequency (thermoelastic signal) was considered as an indicator of material degradation and compared to the data provided by an extensometer. The correlation between thermoelastic and mechanical data allowed to build a new experimental model for evaluating and predicting material stiffness degradation by just using thermoelastic data. The proposed approach seems to be very promising for stiffness degradation assessment of real and complex mechanical components subjected to actual loading conditions.

Nomenclature

E_0, initial Young's modulus (MPa)

E, actual Young's modulus (MPa)

$\frac{E}{E_0}$, Stiffness degradation (MPa/MPa)

$(E/E_0)_{mod}$ stiffness degradation modeled by using thermoelastic data

f,mechanical loading frequency (Hz)

N, actual loading cycles

N_f, total loading cycles

N0, initial loading cycles of a specific thermal sequence

N/N_f ,cycles-to-total cycles ratio

S, thermal signal (Unit Signal)

S_{mean} , mean thermal signal (Unit Signal)

S1, the first amplitude harmonic of thermal signal (thermoelastic signal) (Unit Signal)

S2, the second amplitude harmonic of thermal signal (Unit Signal)

$(S1\_filt)_N/(S1\_filt)_{N0}$,filtered thermoelastic signal evaluated at cycles N normalised by initial cycles N0

$(S1\_98prc)_N/(S1\_98prc)_{N0}$, 98th percentile of thermoelastic signal evaluated at cycles N normalised by initial cycles N0

$(S1\_2prc)_N/(S1\_2prc)_{N0}$, 2nd percentile of thermoelastic signal evaluated at cycles N normalised by initial cycles N0

φ , Phase shift of the first harmonics (rad)

φ_d, phase shift of the second harmonics (rad)

σ_{max} , maximum stress (MPa)

ω, system pulsation (rad/s)

Introduction

Fibre reinforced polymer (FRP) materials are widely exploited in the weight-critical structural applications due to the high strength-to-weight ratio, which allows the advantage of a great fuel saving [1]. Despite this advantage, their intrinsic anisotropy and heterogeneity play a remarkable role in the assessment of mechanical properties by making complex the damage mechanisms [2]. In this regard, residual life and fatigue damage assessment are the prime concerns when the materials or components are subjected to fatigue loading. It follows that, as composites represent primary structural members in various fields of industry (aerospace, automotive...), extensive research campaigns and suitable investigations on in-service components need to be performed [1-3]. In addition, the data analysis requires the knowledge of several typical phenomena (i.e. damage initiation and propagation in layer and at interface regions[4]. In this regard, different approaches have been developed [5-15] to describe the fatigue damage mechanisms based on macroscopic failure, strength degradation, actual damage mechanisms, and stiffness reduction in terms of degradation of elastic properties during fatigue loading. By considering these damage mechanisms, various studies were carried out[18-23] to understand their influence on stiffness degradation that can be described as the ratio of actual Young's modulus (E) and the undamaged modulus (E_0) and depends on the imposed stress (the dependence is a power function)[1], [3], [8-15]. Stiffness degradation of a laminate is caused by transverse cracks and delamination. The matrix cracking is the first mechanism that appears in the plies with transverse fibres when load is applied. Even if, it does not determine a sudden failure, it can be detrimental to the strength as it produces a mechanical properties reduction. Matrix cracking enhances resin-dominated damage modes that involve a local delamination[16]. Matrix cracking and delamination affect the load carrying capability of the material [17], they can also occur sometimes independently and sometimes interactively[9] making difficult any prediction.

Focused on determining the material deterioration, Kobayashi et al.[24], proposed an analytical model for predicting the formation of cracks by considering an average stress distribution for each ply. However, the crack formation is a local phenomenon hence a more local analysis is required to understand its effect on mechanical properties.

Another approach adopted the shear-lag theory[25-28] for describing the effect of micro-cracking and micro-crack induced delamination on material behaviour. The study [28] was focused on isolated cracks while another analytical model [29], overpassed the problem of isolated cracks by considering interacting cracks in any ply of a symmetric laminate.

The computational cost, the assumptions on damage mechanisms and their appearance (isolated, multiple, interacting) make these approaches difficult to be performed. In all the cases, the experimental validation is essential for understanding the real behaviour of the specific material.

Besides analytical approaches, several empirical/semi-empirical methods to study the stiffness degradation of the material have been proposed[30-34]. Crammond et al.[31], proposed an experimental analysis of the

stresses and strains in double butt strap joint in GFRP composite by using digital image correlation that required an accurate speckle pattern painted. Packdel [34], performed optical microscopy to study mechanical properties. In the same way, Hosoi et al.[2], performed the evaluation of inner and outer crack density and delamination by using microscope and soft X-ray tomography while in [35] used ultrasonic C-SCAN for assessing delaminated areas. Chen [36] , measured the mechanical properties variations of a composite wind turbine blade by installing strain gauges. O'Brien et al.[23], proposed a method to predict stiffness loss at failure from a secant modulus criterion by measuring stress by means of strain gages. The technique requires a careful installation and the related measurement is punctual.

All these techniques and methods to evaluate damage parameters require an accurate setup and/or post-mortem inspections to determine the typical damage mechanism present and the number of crack sites.

A full-field technique, capable of providing a map of signal proportional/correlated to material degradation would be suitable for studying material behaviour in laboratory and in-situ on real components. In this way, the thermography has already demonstrated its capability in the assessment of mechanical behaviour of metals[37-39].

In the field of composites, Montesano et al. [33], and Gagel et al. [30], adopted thermography to estimate the strength at specific number of cycles and to determine qualitatively the sites of final failure in fatigue loaded GF-NCF-EP in an early stage of the fatigue life. Even if this technique is useful, it has already been demonstrated that temperature is a parameter influenced by several factors [40].

The Thermoelastic Stress Analysis (TSA) technique can be used to assess the amplitude of the thermal, under adiabatic conditions, that linearly depends on the sum of the principal stresses/strains[37], [40-43]. In this regard, Emery et al.[37], showed qualitatively the possible relationship between the component of thermoelastic signal and the stiffness degradation. The advantage of this approach is such that thermal signal provides full field information related to damage with a simple set-up.

By following this approach, the aim of the research is to present a novel experimental model, based on thermoelastic data, capable of describing the stiffness degradation of a quasi-isotropic composite undergoing fatigue constant amplitude tests.

No similar models based on thermoelastic data have been presented in literature yet. In particular, by correlating mechanical and thermal data at a specific cycles number, material damage state was assessed during the test by means of a contactless technique requiring a simple setup.

The advantage of the proposed approach lies in the possibility to implement the procedure and analysis on in-service structures/components.

Theoretical Framework

2.1 Mathematical Models for stiffness degradation

Residual strength and stiffness are commonly indicated as damage metrics[43]. Depending on loading conditions they decrease through the cycles until achieving a certain critical value which determines the failure of material [43, 44].

Under cyclic loading, the stiffness of the whole fatigue life is characterised by three typical behaviours Fig.1[10,17-18,41]. The first trend lasting roughly 10-20% of the whole life is characterised by inner and outer matrix cracking. This latter produces edge delamination and/or local delamination in the second stage [2]. The appearance of delaminations is the consequence of the achievement of a specific damage state where crack density saturates[27-30]. This phase is characterised by a succession of micromechanics equilibrium stages. It is slow due to the multiplication of cracks in the matrix and the coalescence of delaminations which reduces the rate of damage[34]. In the third phase, a widespread fibres breakage governs the failure of the material.

As the major of stiffness reduction of an off-axis dominated laminate appears from first to second stage, it

becomes interesting to evaluate the amount of mechanical properties loss. Ogin et al.[10], proposed a power dependence between the stiffness reduction rate dE/dN , maximum stress$\sigma_{\mu a \xi}$ and$N$ the cycles to failure at specific$\sigma_{\mu a \xi}$:

$$-\frac{1}{E_0}\frac{\mathrm{dE}}{\mathrm{dN}} = A^*\left(\frac{{\sigma_{\max}}^2}{E^2(1-\frac{E}{E_0})}\right)^{n} \quad (1)$$

where $A*$ and n are material constants andE_0 is the initial Young modulus in undamaged conditions.

By integrating Eq. (1), it is possible to obtain the stiffness reduction expression:

$$\frac{E}{E_0} = 1 - \left[K'^{\frac{1}{n+1}}\left(\frac{{\sigma_{\max}}^2}{{E_0}^2}\right)^{n/(n+1)} (N)^{1/(n+1)}\right] (2)$$

where K' and is a material constant. In a compacted form, as demonstrated by Ogin [10], it becomes:

$$\frac{E}{E_0} = 1 - A\left(\frac{\sigma_{\max}}{E_0}\right)^{b}(N)^{d} (3)$$

The Young's modulus variation, Eq. (3), is a function at the same time of material coefficients A , b , d , the reached cycles and the specific stress level, making complex the prediction of stiffness reduction especially in those applications where imposed stress is unknown.

Another form of stiffness degradation was recently proposed by[3], [17] as a function of cycles-to-total cycles ratioN/N_f :

$$\frac{E}{E_0} = K(\sigma_{\max})\ (\frac{N}{N_f})^{k} (4)$$

where K and k are material constants, and specifically,K depends on imposed stress.

The material coefficients are obtained by fitting the mathematical model to the experimental data and depend on several variables: stacking sequence, ply thickness, material properties, load, and stress ratio[34], [43-44].

2.2 Thermoelastic Stress Analysis technique for composites

In order to study the stiffness degradation, the temperature is particularly promising as it is related to the energy involved in fatigue damaging [39]. In particular, the thermoelastic temperature component is strictly correlated to elastic properties of material [37-39] as it represents the reversible response of the material to the external mechanical excitation under adiabatic conditions. The amplitude of thermoelastic component can be described by the well-known form[37] :

$$T = \frac{-T_0}{\rho C_p}(\alpha_1\sigma_1 + \alpha_2\sigma_2) (5)$$

where T_0 is the environment temperature, $\rho$the density, C_p is the specific heat at constant pressure, a_ι and $\Delta\sigma_\iota$respectively the linear thermal diffusivity and peak-to-peak stress variations in the principal material directions.

Pitarresi et al. [45], modelled the thermoelastic behaviour of a composite where the resin rich layer acted like a strain witness. For outer lamina detected by infrared detector, it is likely that the role of the resin is influent in the stress analysis especially in the first part of loading cycles where, as found by Nijessen[43], stiffness degradation is matrix-driven.

By assuming the laminate is in plane strain conditions, the surface strain field is identical through the thickness. The relation between the peak-to-peak temperature variations and stress amplitude variations under the hypothesis of isotropic resin and adiabatic conditions are [45]:

$$T^r = -T_0\left(\frac{\alpha^r}{\rho^r \mathrm{Cp}^r}\right)\left(\frac{E^r}{E_l^c}\right)\left(\frac{1-v_{\mathrm{lt}}^c}{1-v^r}\right)\left[\sigma_l^c + \left(\frac{E_l^c}{E_t^c}\frac{1-v_{\mathrm{tl}}^c}{1-v_{\mathrm{lt}}^c}\right)\sigma_t^c\right] (6)$$

where upper the script c indicates the composite while $r$the resin contribution to Young's moduli, Poisson's moduli$\upsilon_{\lambda\tau}$, $\upsilon_{\tau\lambda}$, the subscript$l$ stands for longitudinal and t for transverse. Eq. 6 allows the assessment of

the thermoelastic temperature signal of resinΔT^p related to the sum of longitudinal and transverse stress variations$\sigma_l^c + \left(\frac{E_l^c}{E_t^c}\frac{1-v_{\mathrm{tl}}^c}{1-v_{\mathrm{lt}}^c}\right)\sigma_t^c$, through thermo-physical properties of resin$\frac{\alpha^r}{\rho^r \mathrm{Cp}^r}$, T_0, and a combination of Young's and Poisson's moduli ratios$\left(\frac{E^r}{E_l^c}\right)\left(\frac{1-v_{\mathrm{lt}}^c}{1-v^r}\right)$of resin and composite.

Eq. (6) provides a tool for studying the relationship between temperature and stresses and describes a local phenomenon strongly related to mechanical properties variation throughout laminae.

In the case of local damaged areas, the stress values change with respect to the initial conditions. As the damage growths several phenomena appear as described by [41], producing an opposing behaviour in the signal [37]: stiffness/strength variations.

Damage mechanisms can be basically imputable to matrix cracking of off-axis laminae [44] due to Poisson's ratio mismatch between plies and a shear mismatch at interfaces. The appearance of a transverse crack involves the change of the cross-section area with the consequent changes of stress distributions and the reduction of the load carrying capability[8],[37]. Moreover, in the lamina several zones are interested by higher stress values and some others by lower stresses.

Due to variety of fatigue mechanisms occurring in the material and their random appearance that affects locally certain regions of material, a great advantage of using thermoelastic stress analysis would be to assess a parameter leading a local analysis.

Material and Methods

The samples tested in this paper were obtained by Automated Fibre Placement technology [46] where robotic system can depose each layer of the laminate with different orientations. Each tape is pressed to the mould by a roller which provides the proper compacting pressure [47].

The specimens were obtained from a panel made of sixteen plies of epoxy-type resin reinforced by carbon fibres with a stacking sequence of $[0/\text{-}45/45/90/90/45/\text{-}45/0]_2$. The panel dimensions were 560 mm (weight) and 695 mm (length) while sample were 25 mm width, 250 mm length and 3.5 mm thick. All the specimens were tested on an INSTRON 8850 (250 kN capacity) a servo-hydraulic loading frame.

Tensile tests were preliminarily performed in order to evaluate the ultimate tensile strength of material (824 MPa, standard deviation 84.57 MPa). The tests were carried out at 1 mm/min of displacement rate according to the Standard [48].

Constant stress amplitude tests were performed (S/N curve, run-out at $2*10^6$ cycles, load control) at stress ratio of 0.1 and at loading frequency of 7 Hz. All the stress levels are reported in Table I in terms of maximum and mean stresses applied. In Table I, the values marked with an asterisk indicate the test with the acquisition of the thermal signal. For each stress level applied reported in Table I, one sample was tested. An extensometer with clamping length of 25 mm was used for strain measurements. The acquisition of stress/strain values from loading system were sampled at 100 Hz. An optical microscope Nikon SLZ1000 was used for post-mortem damage investigations.

Fig. 2a shows the results in terms of *S/N* curve and the 90% prediction interval bounds. The endurance limit at $2*10^6$ cycles was obtained in correspondence of a maximum stress of 482 MPa.

Infrared sequences were acquired by a cooled In-Sb detector FLIR X6540 SC (640X512 pixel matrix array, thermal sensitivity NETD $<$ 30 mK) with a frame rate of 177 Hz. The spatial resolution in terms of millimetre-to-pixel ratio was roughly 0.35. Each thermal sequence contained 1770 frames that corresponds to 170 loading cycles acquired. Temperature and stress/strain data were sampled at the same cycles.

Fig. 2b reports the equipment layout in terms of loading frame and IR detector and Fig. 2c reports the sample and extensometer setup.

Signal Processing

In this section, the algorithms for processing both thermal and mechanical data series are presented to assess the metrics to represent the stiffness reduction of the material. Extensometer provided averaged stress/strain data in the gage length while the analysis of thermal signal provided full field maps with local information as demonstrated in [39].

4.1 Processing of the data provided by extensometer

Mechanical data were processed by using Matlab® software according to the procedure represented in Fig. 3. For each test, the values of the number of cycles N , the force F and displacement $s$allowed the assessment of stress σ and strain ϵ . In particular, for each stress/strain curve, the slope of the elastic trends (conventionally indicated as rising and descending) was calculated automatically by taking into account a minimum of 12 data. Such the analysis provided Young's moduli: $E_{load}$and E_{unload} . For each cycle N , the mean value E of these latter was evaluated and divided to Young's modulus in undamaged condition E_0 , $(E/E_0)_N$. To reduce the noise of the data series a five-points moving average filter was applied to $(E/E_0)_N$ values of the different stress levels.

4.2 Thermal data processing

Thermal sequences provided by the IR camera, were processed according to the procedure presented in [40].

A signal reconstruction algorithm based on the least squares method was performed in order to extract pixel by pixel from the generic thermal signal S , Eq.7, its components:

$$S\left(\frac{N}{f}\right) = S_{\text{mean}}(\frac{N}{f}) + S1\sin\left(\omega\frac{N}{f} + \varphi\right) + S2\cos\left(2\omega\frac{N}{f} + \varphi_d\right) (7)$$

where the S_{mean} is the term describing the mean temperature while *S1* and *S2* are respectively the first and second amplitude harmonics, φ and $\varphi_d$are phase shift of first and second harmonics respectively and the system pulsation is $\omega = 2\pi f$.

In this research, the first amplitude harmonic signal representative of the thermoelastic signal and the related map were considered for the analysis according to the procedure of Fig.4. The first consideration on matrixes in Fig. 4, obtained by frequency domain analysis, is thatS_{mean} does not provide local information [40] while *S1*allows for assessing more local information[39-40]. The algorithm involves the following steps according to Fig. 4:

- the size reduction to the gage length of maps$S1_N$, in order to refer thermoelastic signal to the area controlled by extensometer, the output map is*(S1_red)*$_N$. The subscript N represents the number of cycles at which thermal sequence was recorded. - a 2D median filtering of *(S1_red)*$_N$ maps. Each output pixel represents the median value in a 3-by-3 neighbourhood around the corresponding pixel of the input image,*(S1_filt)*$_N$. - the extraction of the mean value, 98$^{\text{th}}$ and 2$^{\text{nd}}$ percentiles,*(S1_mean)*$_N$, *(S1_98prc)*$_N$ and *(S1_2prc)*$_N$ respectively, to make a preliminary analysis of the behaviour of thermoelastic signal. - the normalization of each *(S1_filt)*$_N$ map by initial value (number of cycles*N0*),*(S1_filt)*$_N$/*(S1_filt)*$_{N0}$. - the extraction of the mean value, 98$^{\text{th}}$ and 2$^{\text{nd}}$ percentiles,*(S1_mean)*$_N$/*(S1_mean)*$_{N0}$, *(S1_98prc)*$_N$/*(S1_98prc)*$_{N0}$and *(S1_2prc)*$_N$/*(S1_2prc)*$_{N0}$respectively. These latter represent the thermal metrics used for evaluating the damage. The use of percentile instead of maximum/minimum values allows to avoid outliers in the analysis.

In Fig. 5, the evolution of percentiles and mean values of thermoelastic signal *(S1_mean)*$_N$, *(S1_98prc)*$_N$ and *(S1_2prc)*$_N$ are reported. Each test was named as sample/50-60-65-70/% UTS. The index *(S1_98prc)*$_N$, Fig. 5a, presents a variable trend (increasing/decreasing) demonstrating the complexity of damage mechanisms and their effects on composites. Fig. 5b reports the mean values *(S1_mean)*$_N$ which seem more affected by the influence of maximum signal. The signal *(S1_2prc)*$_N$ in Fig. 5c exhibits a decreasing behaviour through the cycles that is reproducible for each test. This latter parameter seems to be more robust to follow the stiffness degradation than others as confirmed by the analysis of[37].

Results

5.1 Stiffness degradation obtained by extensometer

In Fig. 6, the data from extensometer processed according to the algorithm of section 4.1, are presented.

Fig. 6a shows E/E_0 versus N . At a first sight, it is possible to see that the entity of stiffness reduction is the same at each stress level, and the metrics achieves a steady-state value of 0.80 for each test. At a specific ratio value ofN/N_f , Fig. 6b, all the data exhibits the same value of E/E_0 and present a steady state condition. The stiffness reduction occurs up toN/N_f of 0.3 according to literature[10], [17].

The stress dependence is appreciable in Fig. 6a, but at fixedN/N_f there is a slight effect on stiffness reduction.

In this research, the models of literature (Eq. (3) and (4)) have been considered as a reference for analysing the stiffness loss trend.

Table IIa reports the coefficients A , b , d of Eq. (3) obtained by the fitting of the data provided by extensometer and the squared correlation coefficient R^2 .

Eq. (4) can be rewritten by indicating the stress dependence of Kcoefficient, Eq. (8):

$$\frac{E}{E_0} = (C\sigma_{\max})^a \left(\frac{N}{N_f}\right)^k \quad (8)$$

with the coefficients C , a and k experimentally determined.

Table IIb reports the coefficients of Eq. (8) together with theR^2 coefficient. This latter is higher in the case of the model described by Eq. (8) indicating a better capability of this model in describing the stiffness degradation of the investigated material.

Fig. 7 reports graphically for each stress level the comparison between the two models and experimental data in terms ofE/E_0 . The model of Eq. (8) (black dotted line) fits better than the one of Eq. (3) (black solid line) the experimental data. However, it is noteworthy to highlight that all the literature models are not capable of describing all the damage stages of the materials. In effect, the steady state conditions are not taken into account in the model even if the stabilisation of the stiffness is an important stage of the damage [5-15].

The model of Eq. (3) fits very well the behaviour of the material at initial cycles but in some cases (Fig. 7a and c) it does not model the major stiffness degradation that occurs between 0-0.4 ofN/N_f . On the other hand, the model of Eq. (8) seems to be a good compromise for describing all the damage stages. This latter model will be used as reference to represent stiffness degradation of the material in the next section.

5.2 Thermoelastic Data

In this section, the data processed according to the procedure indicated in section 4, are presented.

Fig. 8 reports for three imposed stress values, the$(S1_filt)_N$ /$(S1\_filt)_{N0}$ normalised thermoelastic signal values.

The sample at 50%UTS exhibits a widespread lower signal except in some localised areas where the signal is high in presence of the transverse cracks. The samples at 60-65%UTS, at the sameN/N_f value present a similar behaviour of the thermoelastic signal. In this case, the thermoelastic maps present a more evident effect of the transverse cracks due to the higher values of the imposed stress.

By resuming, the normalised thermoelastic maps at the initial stage of the test present a characteristic behaviour related to the stress/strain of the laminate, as previously described. During the cycles, the damage produced by the transverse cracks determines a stress/strain redistribution within laminae that, in turn, leads to a stress/strain increase or decrease with respect to initial conditions. It follows that, the thermoelastic signal increases in correspondence of the cracks and decreases in the rest of the gage area due to the reduction of the load carrying capability of the laminate. In this regard, the minimum thermoelastic signal (2^{nd} percentile) was adopted as the proper metrics for describing the stiffness degradation.

5.3 Modelling the stiffness degradation by using Thermoelastic Data: A calibration by using mechanical data

Fig. 9a reports the $(S1\_2prc)_N / (S1\_2prc)_{N0}$ data plotted versus N while in Fig. 9b, the data are compared in terms of N/N_f . In Fig. 9a, the thermoelastic data show a stress dependence from lower to higher imposed stress. Such stress effect is slight when data are compared in terms of N/N_f , Fig. 9b.

By observing both Fig. 9a-b, it appears that mechanical and thermal data follow the same trend. In particular, the thermoelastic signal metrics exhibits a steady state from N/N_f =0.4 at a value of 0.4. (Unit Signal/ Unit Signal).

In Fig. 10, the data of E/E_0 and $(S1\_2prc)_N / (S1\_2prc)_{N0}$ are reported in the same plot for each test as function of N/N_f . The extensometer data in terms of E/E_0 have been opportunely sampled, in order to compare mechanical and thermal data at the same N/N_f values. In Fig.10a-b-c-d, a slightly higher sensitivity of thermoelastic data than mechanical data is observed: for each stress level the initial stiffness loss described by $(S1\_2prc)_N / (S1\_2prc)_{N0}$ is characterised by a more severe decrease. This can be attributed to the fact that the thermoelastic signal provides a local information of the behaviour if compared to the mean value of the stiffness provided by extensometer.

The following step was the correlation of thermal and mechanical data at fixed N/N_f values. By using for $(S1\_2prc)_N / (S1\_2prc)_{N0}$ the same mathematical model used for E/E_0 , we obtain Eq. (9):

$$\frac{(S1\_2\mathrm{perc})_N}{(S1\_2\mathrm{perc})_{N0}} = (C'\sigma_{\max})^{a'} \left(\frac{N}{N_f}\right)^{b'} \quad (9)$$

where the symbols a' , b' and C' are empirical constants.

By including Eq. (9) in Eq.(8), a direct relation between E/E_0 and $(S1\_2prc)_N / (S1\_2prc)_{N0}$ can be obtained, Eq.(10).

$$\left(\frac{E}{E_0}\right)_{\mathrm{mod}} = (C\sigma_{\max})^{a} \left(\frac{1}{C'\sigma_{\max}}\right)^{a'k/b'} \left(\frac{(S1\_2\mathrm{perc})_N}{(S1\_2\mathrm{perc})_{N0}}\right)^{k/b'} = A \left(\frac{(S1\_2\mathrm{perc})_N}{(S1\_2\mathrm{perc})_{N0}}\right)^{b} \quad (10)$$

Eq. (10) represents a mathematical relation between stiffness degradation and thermoelastic signal. It shows also that to obtain E/E_0 values from thermoelastic data one can:

- To find the coefficients A and b indirectly estimating a , k , a' , b' , C , C' .
- To find A' and 'b' directly by plotting E/E_0 versus $(S1\_2prc)_N / (S1\_2prc)_{N0}$.

The coefficients are reported in Table III for each stress level. They are slightly similar at each stress level, as confirmed by the experimental data (both mechanical and thermal), Fig.11.

In Fig. 11, for each stress level the E/E_0 data are reported compared to $(S1\_2prc)_N / (S1\_2prc)_{N0}$ data. Specifically, in Fig.11a-b, the high number of acquired data close to the value 0.80 of E/E_0 , is due to the presence of a plateau of stiffness degradation. The test run at the stress level of 70%UTS, Fig. 11d, is the one with a smaller number of thermal acquisitions, but they are well distributed for each value of E/E_0 .

An advantage of the present material is such that it does not present a marked stress dependence when the metrics E/E_0 and $(S1\_2prc)_N / (S1\_2prc)_{N0}$ are compared to N/N_f . So, in order to describe the material behaviour one can choose the coefficients $'A'$ and 'b' of a specific stress level from Table III. If the test at 70%UTS is adopted as representative of the relation between thermal and mechanical data, the model is:

$$\left(\frac{E}{E_0}\right)_{\mathrm{mod}} = 1.01 \left(\frac{(S1\_2\mathrm{perc})_N}{(S1\_2\mathrm{perc})_{N0}}\right)^{0.22} \quad (11)$$

In the next section, the validation of the model for the data at different stress levels will be performed and an estimation of errors between measured data and modelled data is provided.

Discussion

In this section $(E/E_0)_{mod}$ values obtained by Eq. (11) have been expressed as a function of N/N_f by using a power law in of Eq. (4) where the coefficient depending from stress $K(\sigma_{\max})$ is 0.81 and the exponent k is -0.03.

In Fig.12 are reported for each stress level, the experimental data compared with the models according to Eq. (3)-(8) and the model obtained by calibrating thermoelastic data $(E/E_0)_{mod}$.

The results in Fig. 12 show a promising correlation between the stiffness degradation obtained from thermoelastic data-based model and extensometer data. In particular, at stress levels higher than the endurance limit (Fig. 12b-c-d) the $(E/E_0)_{mod}$ data match the experimental data at the steady state better than the other models.

The capability of the proposed approach can be also assessed by evaluating absolute errors between the values forecast by each model and experimental data (E/E_0), at each stress level in terms of maximum stress:

$$\text{Absolute Error}_1 = \left| \left(\frac{E}{E_0}\right)_{Eq.3} - \left(\frac{E}{E_0}\right)_{\frac{N}{N_f}} \right|_{\sigma_{\max}} \quad (12)$$

$$\text{Absolute Error}_2 = \left| \left(\frac{E}{E_0}\right)_{Eq.8} - \left(\frac{E}{E_0}\right)_{\frac{N}{N_f}} \right|_{\sigma_{\max}} \quad (13)$$

$$\text{Absolute Error}_3 = \left| \left(\frac{E}{E_0}\right)_{\text{mod}} - \left(\frac{E}{E_0}\right)_{\frac{N}{N_f}} \right|_{\sigma_{\max}} \quad (14)$$

where $(E/E_0)_{Eq.3}$,$(E/E_0)_{Eq.8}$, $(E/E_0)_{mod}$ are respectively the stiffness degradation modelled using Eq.(3), Eq.(8) for just mechanical data and Eq. (11) for thermoelastic data.

The results reported in Fig.13b demonstrate as the model described by Eq.(8) reproduces in a better way the experimental behaviour at specific stress level if compared to the model of Eq. (3), Fig.13a.

In the case of Fig.13b, the absolute error reduces as N/N_f increases while is it is high at initial cycles.

Fig.13c represents the absolute error evaluated between the values of $(E/E_0)_{mod}$ and experimental data. The *Absolute Error*$_3$ is comparable with the other two estimated errors specifically, it is generally lower than *Absolute Error*$_1$. This demonstrates the capability of thermoelastic data in describing the stiffness degradation of the material.

Conclusions

In the present work, the stiffness reduction of a quasi-isotropic CFRP laminate obtained by automated fibre placement innovative process was studied by means of a thermographic approach.

A total of ten specimens were tested at four different stress levels, 50-60-65-70% of UTS, and monitored by using infrared thermal camera.

The analysis of thermal signal provided the thermoelastic signal used as metrics for evaluating stiffness degradation. At the same cycles-to-total cycles ratio, thermoelastic data were compared to the data of the extensometer that provided averaged stress/strain data in the gage length of the sample.

Specific processing algorithms were used to extract the mechanical and thermal metrics.

The major outcome of the present research is represented by the modelling of the stiffness degradation by using thermoelastic data.

The other results achieved by performing present research are:

- A demonstration of the capability of the thermoelastic signal to provide local information and making possible the quantitative estimation of the damage in the material.
- A demonstration of narrow correlation between mechanical and thermal behaviour
- A qualitative major capability of the thermoelastic metrics for describing mechanical properties variations

This approach is useful also because it can be adopted to estimate stiffness degradation on in-situ applications on operating components where stress state and damage behaviour are unknown and where the extensometer cannot be used.

Acknowledgements

The authors would like to thank Novotech Aerospace Advanced Technology S.R.L. for the manufacturing of the samples and Professor Riccardo Nobile and Mr. Andrea Saponaro for the support during the experimental activity performed in this work.

References

1. Carvani-farahani A, shirazi A. A Fatigue Damage Model for (0/90) FRP Composites based on Stiffness Degradation of 0° and 90° Composite Plies. J. Reinf. Plast. Compos. 2007; 26 (13).
2. Hosoi A, Sato N, Kusumoto Y, Fujiwara K, Kawada H. High-cycle fatigue characteristics of quasi-isotropic CFRP laminates over 108 cycles (Initiation and propagation of delamination considering interaction with transverse cracks). Int J of Fatigue. 2010; 32:29–36.
3. Degrieck J, Van Paepegem W. Fatigue damage modeling of fibre-reinforced composite materials: Review. Appl Mech Rev.2001; 54(4).
4. Mohammadi B, Fazlali B, Salimi-Majd D. Development of a continuum damage model for fatigue life prediction of laminated composites. Composites: Part A 93. 2017:163–176.
5. Sendeckyj GP. Life prediction for resin-matrix composite materials. In: Reifsnider KL Ed: Fatigue of composite materials. Composite Material Series 4. Elsevier. 1990; 431–483.
6. Shirazi A, Varvani-Farahani A. A Stiffness Degradation Based Fatigue Damage Model for FRP Composites of $(0/\vartheta)$ Laminate Systems. Appl Compos Mater. 2010; 17:137–150.
7. Berthelot J, ElMahi A, LeCorre DJF. Development of transverse cracking in cross-ply laminates during fatigue tests. Compos Sci Technol. 2001; 61:1711–1721.
8. Poursartip A. The Fatigue Damage Mechanics of a Carbon Fibre Composite Laminate: I–Development of the Model. Compos. Sci. Technol. 1986;25:193-218
9. Reifsnider KL, Case S, Duthoit J. The mechanics of composite strength evolution. Comp Sci Tech.2000;60: 2539-2546.
10. Ogin SL, Smith PA, Beaumont PWR. Matrix Cracking and Stiffness Reduction during the Fatigue of a (0/90)s GFRP Laminate. Compos. Sci. Technol. 1985;22:23-31.
11. Stens C, Middendorf P. Computationally efficient modelling of the fatigue behaviour of composite materials. Int J of Fatigue. 2015;80:69–75.
12. Schaff JR, Davidson BD. Life prediction methodology for composite structures. Part I – constant amplitude and two-stress level fatigue. J Compos Mater. 1997;31(2):128–57.
13. Reifsnider KL, Henneke EG, Stinchcomb W, Duke JC. Damage mechanics and NDE of composite laminates. Mechanics of composite mater. New York: Pergamon Press. 1983. p. 399–420.
14. Highsmith A, Reifsnider KL. Stiffness-reduction mechanisms in composite laminates. Damage in composite materials. Philadelphia and PA: ASTM; 1982. p. 103–17.
15. Daniel IM, Lee JW, Yaniv G. Damage Mechanisms and stiffness degradation in grahite/epoxy composites. In: proc. 6th International Conference on Composite Materials and 2nd European Conference on Composite Materials, 1987, pp. 4.129-4.138.
16. Kashtalyan M, Soutis C. Stiffness degradation in cross-ply laminates damaged by transverse cracking and splitting Composites: Part A. 2000;31:335–351.
17. Ospina Cadavid M, Al-Khudairi O, Hadavini H, Goodwin D, Liaghat GH. Experimental Studies of Stiffness Degradation and Dissipated Energy in Glass Fibre Reinforced Polymer Composite under

Fatigue Loading. Polymers and Polymer Composites.2017;25(6):435-446.
18. Okabe T, Onodera S, Kumagai Y, Nagumo Y. Continuum damage mechanics modeling of composite laminates including transverse cracks. Int. J Damage Mechanics. 2017; 0(0): 1–19.
19. Allen DH, Harris CE and Groves SE . A thermomechanical constitutive theory for elastic composites with distributed damage – Part I: Theoretical development. International Journal of Solids and Structures. 1987; 23(9): 1301–1318.
20. Allen DH, Harris CE and Groves SE .A thermomechanical constitutive theory for elastic composites with distributed damage – Part II: Application to matrix cracking in laminated composites. International Journal of Solids and Structures. 1987; 23(9): 1319–1338.
21. Berthelot JM . Transverse cracking and delamination in cross-ply glass-fiber and carbon-fiber reinforced plastic laminates: Static and fatigue loading. App Mech Rev. 2003; 56(1): 111–147.
22. Gudmundson P, Zang W. An analytic model for thermoelastic properties of composite laminates containing transverse matrix cracks. Int. J Solids Struct. 1993; 30(23): 3211–3231.
23. O'Brien TK, Reifsnider KL. Fatigue damage evaluation through stiffness measurements in boron-epoxy laminates. J. Compos. Mater. 1981;15: 55–70.
24. Kobayashi S, Ogihara S and Takeda N. Damage mechanics analysis for predicting mechanical behaviour of general composite laminates containing transverse cracks. Advances in Composite Materials. 2000; 9(4): 363–375.
25. Nairn JA, Hu S. The Initiation and Growth of Delaminations Induced by Matrix Microcracks in Laminated Composites. Int. J Fracture. 1992; 57:1-24.
26. Han YM, Hahn HT. Ply cracking and property degradations of symmetric balanced laminates under general in-plane loading. Composites Science and Technology 1989;35:377–97.
27. Lee JW, Daniel IM. Progressive cracking of crossply composite laminates. Journal of Composite Materials 1990; 24:1225–43.
28. Dharani LR, Tang H. Micromechanics characterization of sublaminate damage Int. J. Fract.1990; 46:123.
29. Carraro PA, Quaresimin M.A stiffness degradation model for cracked multidirectional laminates with cracks in multiple layers. Int J Solids Struct. 2015; 58:34–51
30. Gagel A, Lange D, Schulte K. On the relation between crack densities, stiffness degradation, and surface temperature distribution of tensile fatigue loaded glass-fibre non-crimp-fabric reinforced epoxy. Composites: Part A. 2006; 37: 222–228
31. Crammond G, Boyd SW, Dulieu-Barton JM. Evaluating the localised through-thickness load transfer and damage initiation in a composite joint using digital image correlation. Composites: Part A.2014; 61:224–234.
32. Goidescu C, Welemane H, Garnier C, Fazzini M, Brault R, et al. Damage investigation in CFRP composites using fullfield measurement techchniques: combination of digital image stereo-correlation, infrared thermography and X-ray tomography. Composites Part B: Engineering. 2013;48:95-105.
33. Montesano J, Bougherara H, Fawaz Z. Application of infrared thermography for the characterization of damage in braided carbon fiber reinforced polymer matrix composites. Composites: Part B. 2014;60:137–143
34. Pakdel H, Mohammadi B. Stiffness degradation of composite laminates due to matrix cracking and induced delamination during tension-tension fatigue. Eng Fract Mech. 2019;216.
35. Poursartip A. The Characterisation of delamination growth in laminates under fatigue loading. In: Proc. ASTM Symposium on Toughened Composites. Houston, March, 1985.
36. Chen X. Experimental observation of fatigue degradation in a composite wind turbine blade. Comp Struct. 2019; 212: 547–551.
37. Emery TR, Dulieu-Barton JM. Thermoelastic Stress Analysis of damage mechanisms in composite materials. Composites: Part A.2010; 41:1729–1742
38. Emery TR, Dulieu-Barton JM, Earl JS, Cunningham PR. A generalised approach to the calibration of orthotropic materials for thermoelastic stress analysis. Comp Sci Tech. 2008; 68: 743-752.
39. Palumbo D, De Finis R, Demelio PG, Galietti U. A new rapid thermographic method to assess the

fatigue limit in GFRP composites. Composites Part B: Engineering. 2016;103: 60-67.
40. De Finis R, Palumbo D, Galietti U. A multianalysis thermography-based approach for fatigue and damage investigations of ASTM A182 F6NM steel at two stress ratios. Fatigue Fract Eng Mater. Struct.2019; 42, (1):267-283.
41. Huanga J. Pastor MJ, Garnier C, Gonga XJ. A new model for fatigue life prediction based on infrared thermography and degradation process for CFRP composite laminates. Int J Fatigue.2019; 120:87–95.
42. De Finis R, Palumbo D, Galietti U. Mechanical behaviour of stainless steels under dynamic loading: An investigation with thermal methods. J of Imaging, 2016;2(4):32
43. Nijssen RPL. Fatigue Life Prediction and Strength Degradation of Wind Turbine Rotor Blade Composites. The Netherlands: Knowledge Centre Wind turbine Materials and Constructions (KC-WMC), 2006, p. 93.
44. Whitworth HA. Evaluation of the residual strength degradation in composite laminates under fatigue loading. Composite Structures.2000;48:261-264.
45. Pitarresi G, Found MS, Patterson EA. An investigation of the influence of macroscopic heterogeneity on the thermoelastic response of fibre reinforced plastics. Comp Sci Tech.2005; 65: 269–280
46. Belnoue, JPH, Mesogitis T.Understanding the buckling behaviour of steered tows in Automated Dry Fibre Placement (ADFP) placement pre-preg laminates. Composites: Part A. 2017; 102:196–206.
47. Belhaj M, Deleglise M. Dry fiber automated placement of carbon fibrous preforms. Composites: Part B 50.2013:107–111.
48. Standard test method for tension-tension fatigue of polymer matrix composite materials D3479M-96

Figures and Tables

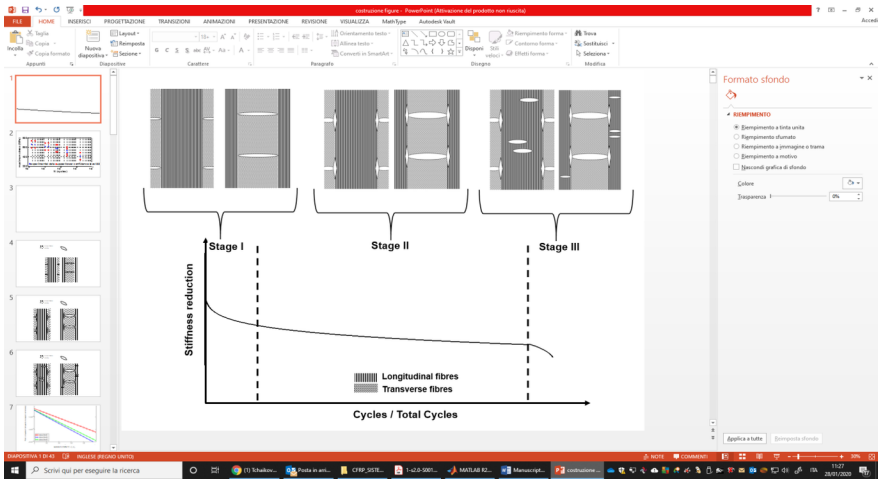

Fig. 1. Typical behavior of a laminate containing both longitudinal and transverse plies, during fatigue

Hosted file

`image2.emf` available at https://authorea.com/users/176512/articles/436282-evaluation-of-damage-in-composites-by-using-thermoelastic-stress-analysis-a-promising-technique-to-assess-the-stiffness-degradation

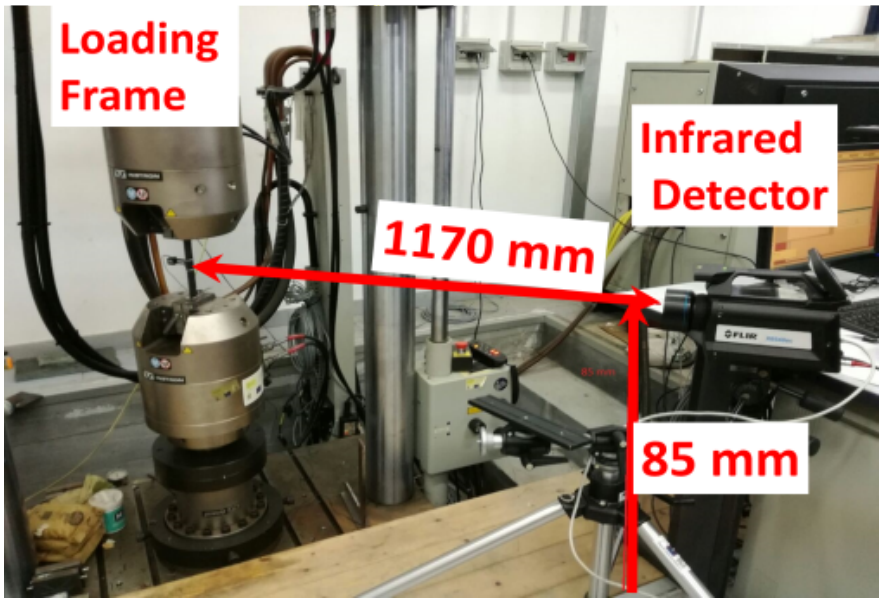

(a) (b)

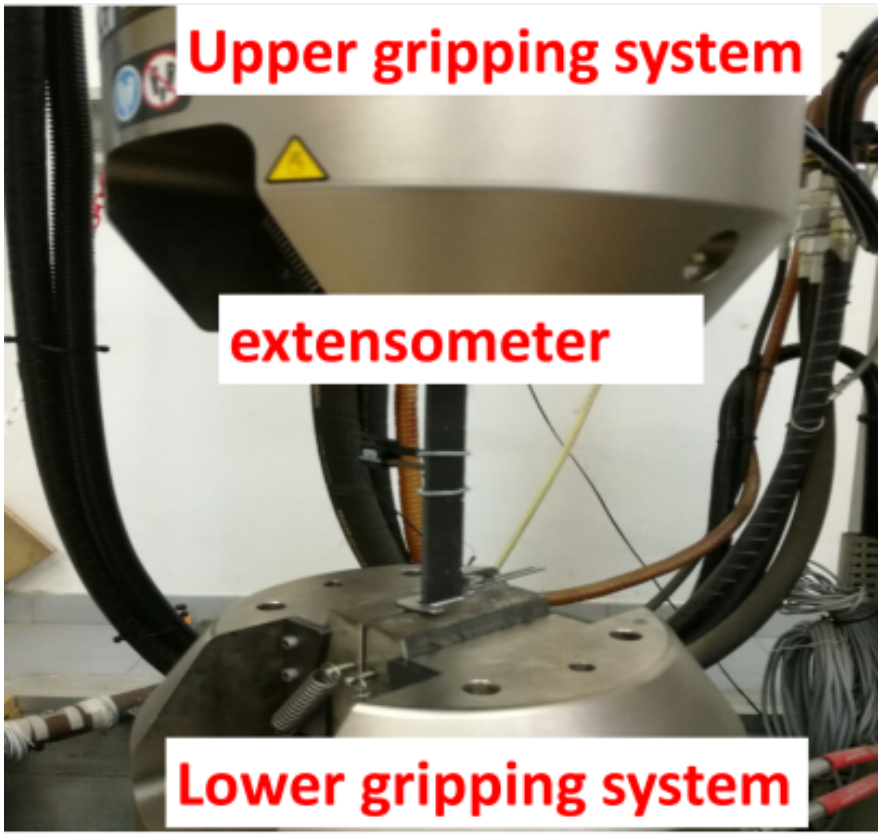

(c)

Fig. 2. (a) S/N curve, (b) equipment and layout (c) details of setup.

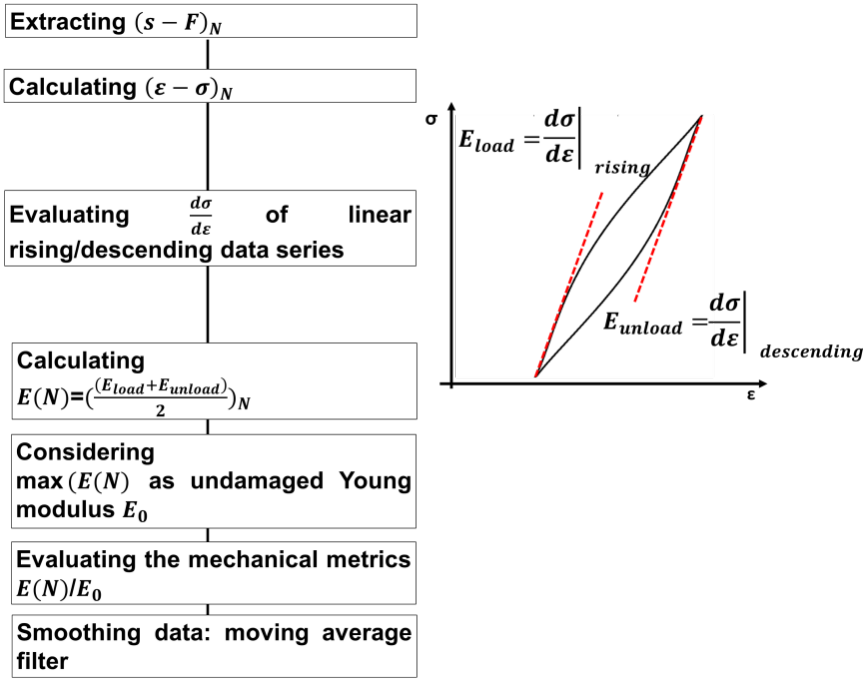

Fig. 3. Procedure for analyzing data from extensometer

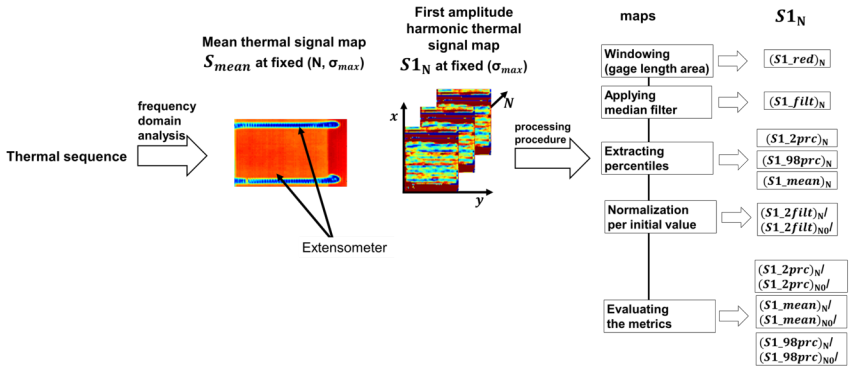

Fig. 4. Procedure for analyzing thermoelastic data

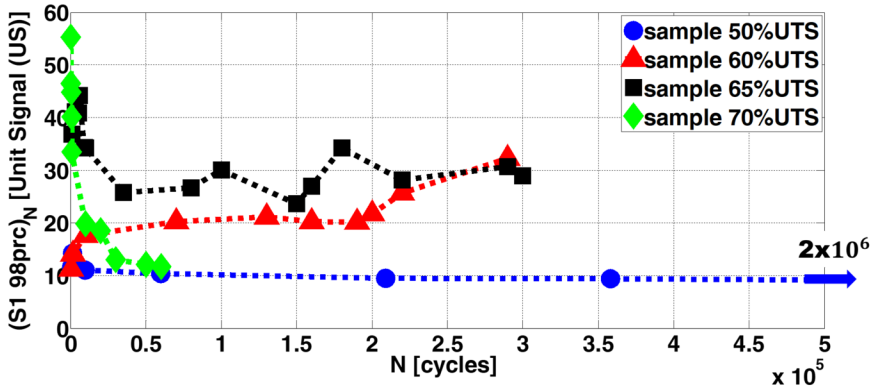

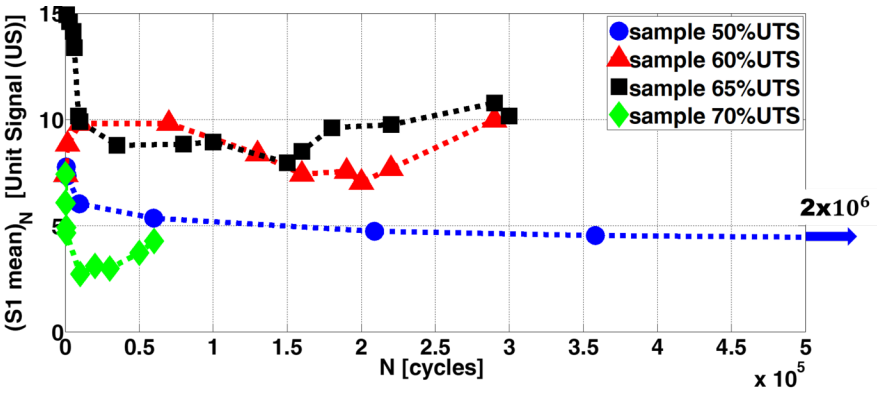

(b)

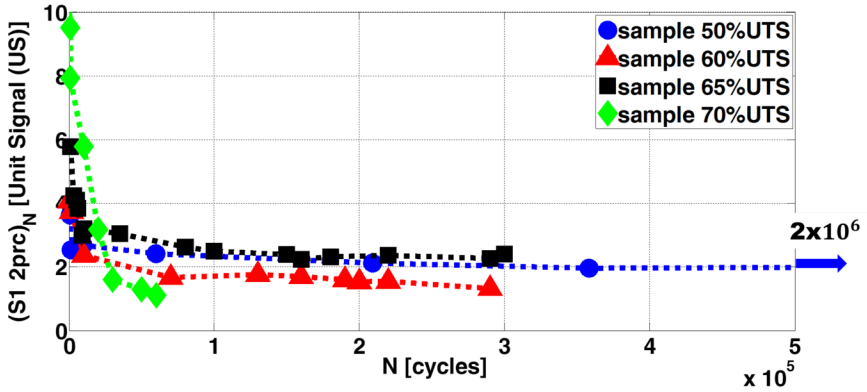

(c)

Fig. 5. (a) Maximum $(S1\_98prc)_N$, (b) Mean $(S1\_mean)_N$, (c) Minimum $(S1\_2prc)_N$, values of thermoelastic signal

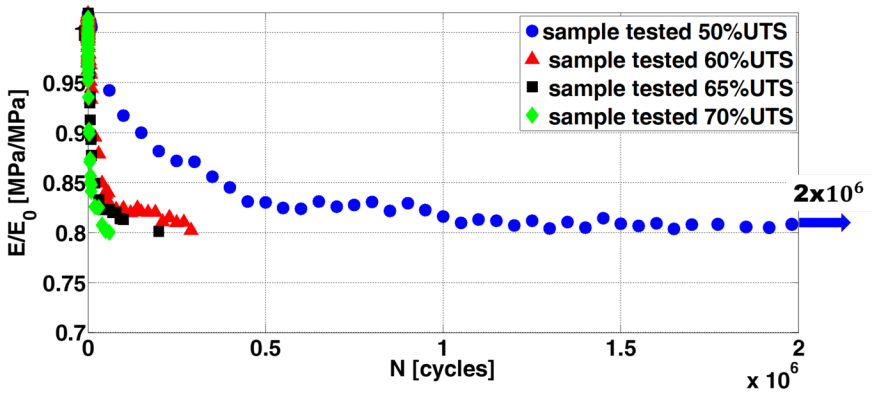

Hosted file

`image11.emf` available at https://authorea.com/users/176512/articles/436282-evaluation-of-damage-in-composites-by-using-thermoelastic-stress-analysis-a-promising-technique-to-assess-the-stiffness-degradation

(a) (b)

Fig. 6. E/E_0 Experimental data (a) versus cycles, (b) versus N/N_f

Hosted file

`image12.emf` available at https://authorea.com/users/176512/articles/436282-evaluation-of-damage-in-composites-by-using-thermoelastic-stress-analysis-a-promising-technique-to-assess-the-stiffness-degradation

Hosted file

`image13.emf` available at https://authorea.com/users/176512/articles/436282-evaluation-of-damage-in-composites-by-using-thermoelastic-stress-analysis-a-promising-technique-to-assess-the-stiffness-degradation

(a) (b)

Hosted file

`image14.emf` available at https://authorea.com/users/176512/articles/436282-evaluation-of-damage-in-composites-by-using-thermoelastic-stress-analysis-a-promising-technique-to-assess-the-stiffness-degradation

Hosted file

`image15.emf` available at https://authorea.com/users/176512/articles/436282-evaluation-of-damage-in-composites-by-using-thermoelastic-stress-analysis-a-promising-technique-to-assess-the-stiffness-degradation

(c) (d)

Fig. 7. $'E/E_0'$ experimental data versus empirical models (a) 50%UTS (b) 60%UTS (c) 65%UTS (d) 70%UTS

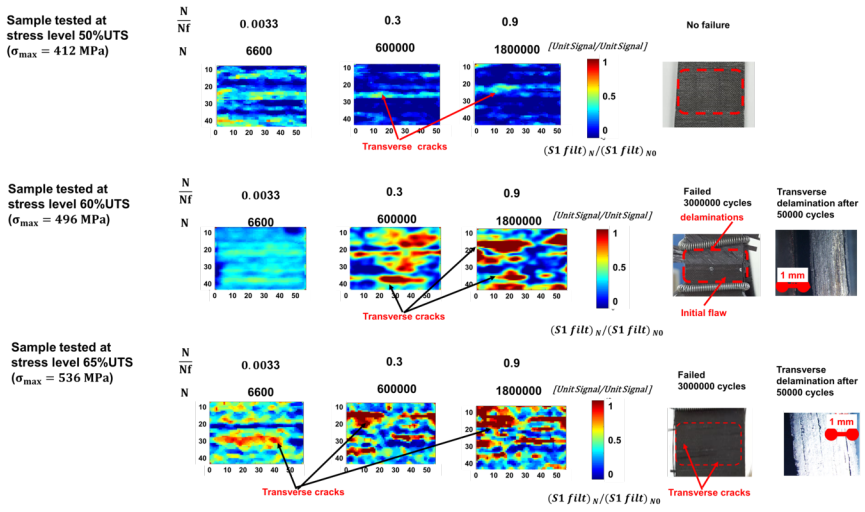

Fig. 8 Qualitative analysis of thermoelastic signal maps$'(S1_filt)_N/(S1_filt)'_{N0}$ for three stress levels.

Hosted file

`image17.emf` available at https://authorea.com/users/176512/articles/436282-evaluation-of-damage-in-composites-by-using-thermoelastic-stress-analysis-a-promising-technique-to-assess-the-stiffness-degradation

Hosted file

`image18.emf` available at https://authorea.com/users/176512/articles/436282-evaluation-of-damage-in-composites-by-using-thermoelastic-stress-analysis-a-promising-technique-to-assess-the-stiffness-degradation

(a) (b)

Fig. 9. $'(S1_2prc)_N/(S1_2prc)'_{N0}$thermoelastic data versus (a) cycles, (b) 'N/N_f'.

Hosted file

`image19.emf` available at https://authorea.com/users/176512/articles/436282-evaluation-of-damage-in-composites-by-using-thermoelastic-stress-analysis-a-promising-technique-to-assess-the-stiffness-degradation

Hosted file

`image20.emf` available at https://authorea.com/users/176512/articles/436282-evaluation-of-damage-in-composites-by-using-thermoelastic-stress-analysis-a-promising-technique-to-assess-the-stiffness-degradation

(a) (b)

Hosted file

`image21.emf` available at https://authorea.com/users/176512/articles/436282-evaluation-of-damage-in-composites-by-using-thermoelastic-stress-analysis-a-promising-technique-to-assess-the-stiffness-degradation

Hosted file

image22.emf available at https://authorea.com/users/176512/articles/436282-evaluation-of-damage-in-composites-by-using-thermoelastic-stress-analysis-a-promising-technique-to-assess-the-stiffness-degradation

(c) (d)

Fig. 10. $'(S1\_2prc)_N/(S1\_2prc)'_{N0}$ and$'E/E'_0$ at fixed 'N/N$_f$ ' for samples: (a) 50%UTS (b) 60%UTS (c) 65%UTS (d) 70%UTS

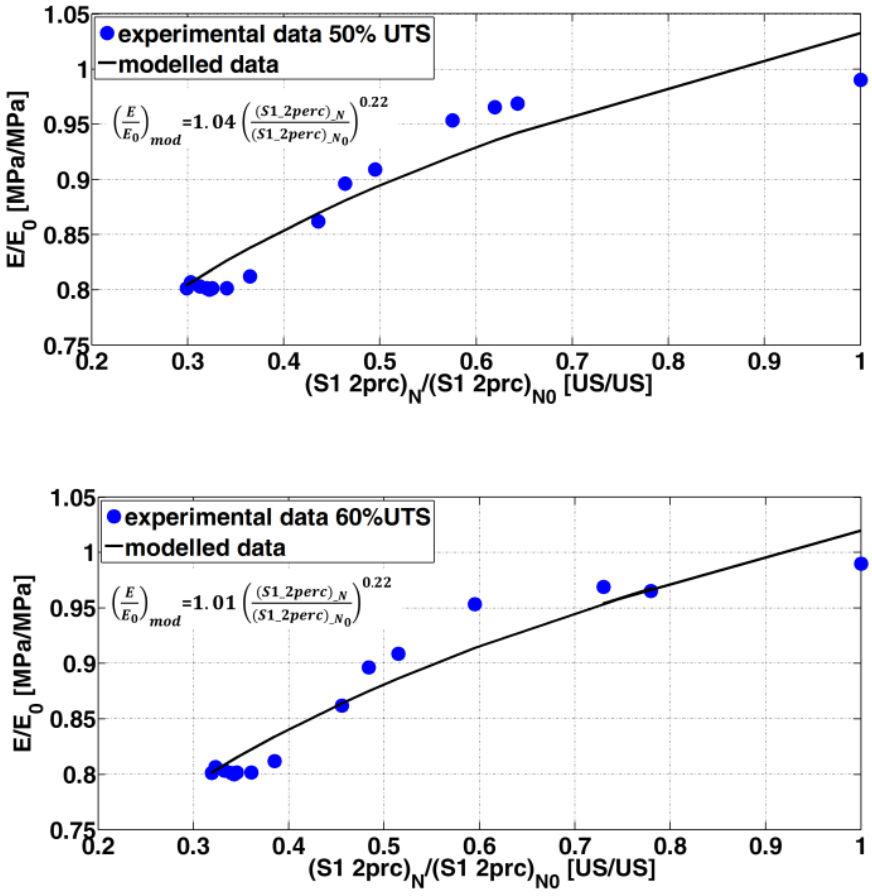

(a) (b)

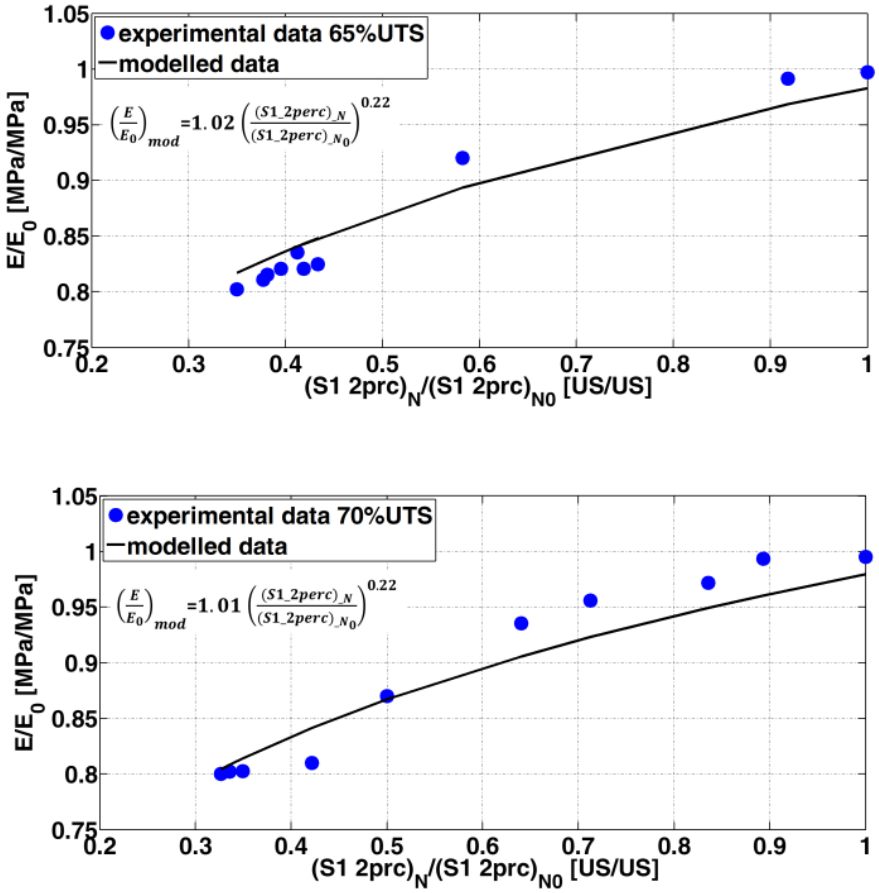

(c) (d)

Fig. 11. $'\frac{E'}{E}_0$ versus$'(S1_2prc)_N/(S1_2prc)'_{N0}$ data and data fitting (solid line) for each stress level.

Hosted file

`image27.emf` available at https://authorea.com/users/176512/articles/436282-evaluation-of-damage-in-composites-by-using-thermoelastic-stress-analysis-a-promising-technique-to-assess-the-stiffness-degradation

Hosted file

`image28.emf` available at https://authorea.com/users/176512/articles/436282-evaluation-of-damage-in-composites-by-using-thermoelastic-stress-analysis-a-promising-technique-to-assess-the-stiffness-degradation

(a) (b)

Hosted file

`image29.emf` available at https://authorea.com/users/176512/articles/436282-evaluation-of-damage-in-composites-by-using-thermoelastic-stress-analysis-a-promising-technique-to-assess-the-stiffness-degradation

Hosted file

image30.emf available at https://authorea.com/users/176512/articles/436282-evaluation-of-damage-in-composites-by-using-thermoelastic-stress-analysis-a-promising-technique-to-assess-the-stiffness-degradation

(c) (d)

Fig. 12. Comparison between experimental data and modeled data at (a) 50%UTS (b) 60%UTS (c) 65%UTS (d) 70%UTS .

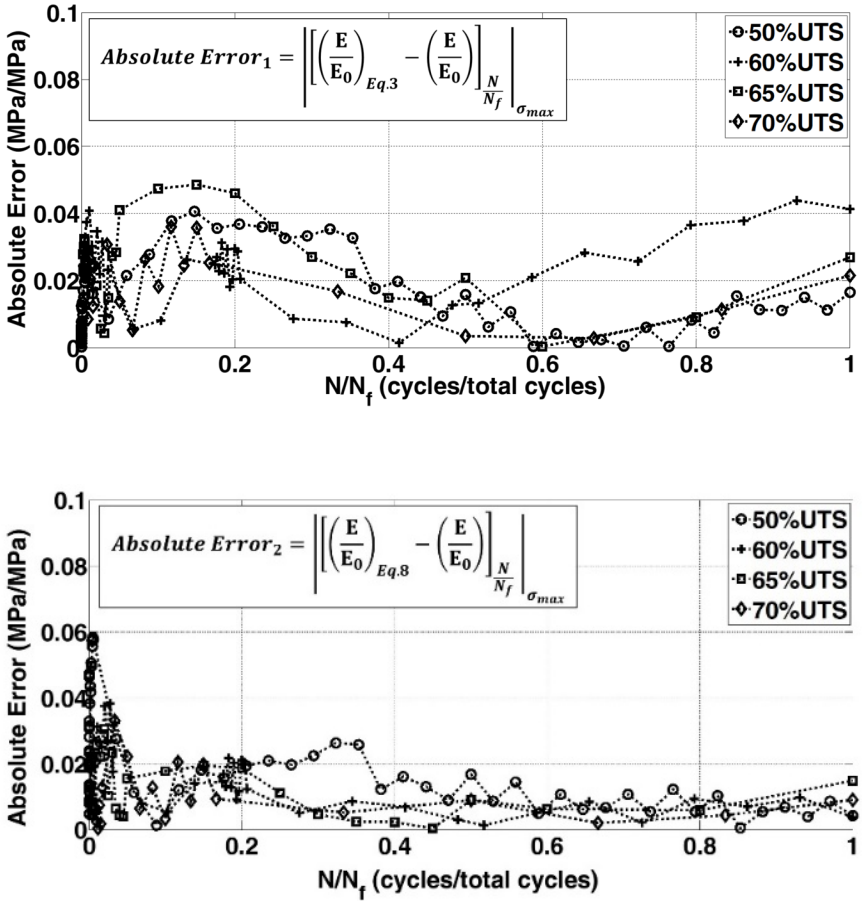

(b)

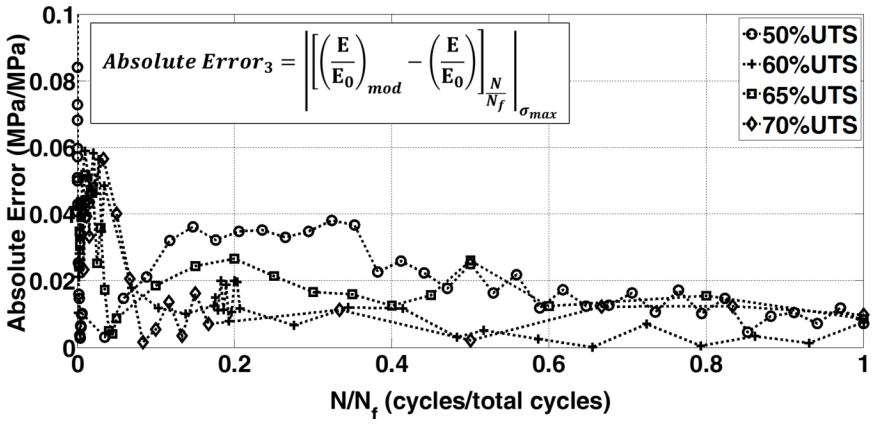

(c)

Fig. 13. Errors between experimental data and models: (a) Eq. (12), (b) Eq. (13), (c) Eq.(14).

Table I. Loading table (stress values rounded up to the nearest unit)

Sample	%UTS	σ_μεαν [ΜΠα]	σ_μαξ [ΜΠα]	N Cycles to Failure	Sample	%UTS	σ_μεαν [ΜΠα]	σ_μαξ [ΜΠα]	N to Fa
1	80%	363	661	1765	6	*65%	295	537	29
2	80%	363	661	2875	7	75%	341	620	65
3	*70%	318	578	60041	8	75%	341	620	12
4	70%	318	578	75461	9	*50%	227	413	2*
5	*60%	273	496	300334	10	50%	227	413	2*

* infrared thermal sequences acquired

Table II. Parameters for mechanical data modeling (a) Eq. (3), (b) Eq. (8).

(a)

UTS %	A [1/cycles]	b	d	E_0 [MPa]	σ_{max} [MPa]	R^2 [/]
50%	19.4	1.53	0.23	69616	413	0.95
60%	14.2	1.59	0.33	87754	496	0.86
65%	13.1	1.62	0.34	92717	536	0.88
70%	19.4	1.70	0.31	59515	577	0.87

(b)

UTS %	C [1/MPa]	a [/]	k [/]	σ_{max} [MPa]	R^2 [/]

50%	0.002	1.66	-0.02	413	0.95
60%	0.002	2.07	-0.04	496	0.97
65%	0.002	1.91	-0.04	536	0.98
70%	0.001	0.39	-0.05	577	0.98

Table III. Coefficients for thermoelastic data calibration by using experimental $'E/E_0'$ data

%UTS	**a** [/]	**k** [/]	**C [1/MPa]**	**a'** [/]	**k'** [/]	**C' [1/MPa]**	**A** [/]	**b** [/]	$\sigma_{\max}$ **[MPa]**
50%	0.36	-0.04	0.001	0.23	-0.21	7.7E-06	1.04	0.22	413
60%	0.45	-0.04	0.001	0.46	-0.21	1.4E-04	1.02	0.22	495
65%	0.27	-0.03	0.001	0.80	-0.17	4.0E-04	1.01	0.22	536
70%	0.68	-0.04	0.001	0.90	-0.17	5.1E-04	1.01	0.22	577